European Journal of Cardio-Thoracic Surgery 49 (2016) 1213–1221
doi:10.1093/ejcts/ezv295 Advance Access publication 9 September 2015

ORIGINAL ARTICLE

Cite this article as: Berdajs D, Mosbahi S, Forro Z, Gerber C, Ferrari E, Charbonnier D *et al*. Numerical analysis of the 3-dimensional aortic root morphology during the cardiac cycle. Eur J Cardiothorac Surg 2016;49:1213–21.

Numerical analysis of the 3-dimensional aortic root morphology during the cardiac cycle

Denis Berdajs[a,*], Selim Mosbahi[a], Zalan Forro[b], Christof Gerber[c], Enrico Ferrari[a], Dominique Charbonnier[d] and Ludwig K. von Segesser[a]

[a] Department of Surgery and Anesthesiology, Cardiovascular Research, University Hospital Lausanne, Lausanne, Switzerland
[b] Swiss Federal Institution of Technology Zürich, Zurich, Switzerland
[c] Department of Anesthesiology, University Hospital of Zürich, Zurich, Switzerland
[d] CFS, Engineering, Lausanne, Switzerland

* Corresponding author. Department of Surgery and Anesthesiology, Cardiovascular Research, University Hospital (CHUV), Rue du Bugnon 46, 1011 Lausanne, Switzerland. Tel: +41-21-3143992; fax: +41-21-3142876; e-mail: denis.berdajs@bluewin.ch (D. Berdajs).

Received 16 April 2015; received in revised form 4 July 2015; accepted 22 July 2015

Abstract

OBJECTIVES: The aim was to define the 3-dimensional (3D) geometrical changes of the aortic root and to determine the local shear stress profile of aortic root elements during the cardiac cycle.

METHODS: Six sonomicrometric crystals (200 Hz) were implanted into the aortic root of five pigs at the commissures and at the aortic root base (AoB). 3D aortic root deformation including volume, torsion and tilt angle were determined. Geometrical data with measured local flow and pressure conditions was used for computed fluid dynamics modelling of the aortic root.

RESULTS: Compared with end-diastole, the sinotubular junction and AoB have maximal expansion at peak ejection: 16.42 ± 6.36 and 7.60 ± 2.52%, and minimal at isovolaemic relaxation: 2.87 ± 1.62 and 1.85 ± 1.79%. Aortic root tilt and rotation angle were maximal at the end of diastole: 17.7 ± 8.8 and 21.2 ± 2.09°, and decreased to 15.24 ± 8.14 and 18.3 ± 0.1.94° at peak ejection. High shear stress >20 Pa was registered at peak ejection at coaptations, and during diastole at the superior two-thirds of the leaflets and intervalvular triangles (IVTs). The leaflet body, inferior one-third of the IVTs and valve nadir were exposed to moderate shear stress (8–16 Pa) during the cardiac cycle.

CONCLUSIONS: Aortic root geometry demonstrates precise 3D changes of tilt and rotation angle. Reduction of angles during ejection results in a straight cylinder with low shear stress that facilitates the ejection; the increase during diastole results in a tilted frustum with elevated shear stress. Findings can be used for comparative analysis of native and synthetic structures with individual compliance.

Keywords: Aortic root • Geometry of the aortic root • Shear stress • Computed fluid dynamics

INTRODUCTION

The aortic root (aortic root) is a complex morphological as well as a functional unit of the three sinuses of Valsava, of three leaflets and three intervalvular triangles (IVTs), and ostia of both coronary arteries [1, 2]. The different shapes of the three sinuses, along with the IVTs create a very complex asymmetrical aortic root shape [1, 3]. This natural asymmetry was validated via 3D geometry that considered direction, tilt angle and the aortic root vector [1, 2]. The impact of the natural aortic root asymmetry on proper valve function, i.e. closure and opening of the aortic valve, however is not known in full detail. In fact, aortic root haemodynamics is complex and includes synchronous morphological deformation of the sinotubular junction (SJ), IVTs, the three sinuses and the aortic root base (AoB) in order to provide a smooth opening and closure of the three leaflets. To date, a majority of studies have focused on sinuses of Valsava and leaflet haemodynamics and, in actuality, little is known about the AoB and IVTs in this complex mechanism. For a long time, it was supposed that the key element of smooth valve movement was the proper functioning of the sinuses of Valsava [4, 5]. The most striking fact, which supports this theory, was the notion of early leaflet deterioration and degeneration following aortic valve implantation in a tubular graft as in the David procedure. The elevated stress shear on the leaflets should induce and lead to early valve degeneration [5–7]. In the recent literature, however, there is strong evidence of excellent long-term results in valve reimplantation with 95% freedom from valve-related complications over 20 years [8, 9].

The aim of this experimental study was to describe aortic root deformation in 3D real time during the cardiac cycle. To accomplish this, a geometrical model of the aortic root was developed and utilized. Experimental data were obtained to create a real-time computed fluid dynamics model to investigate local shear stress, pressure and flow modalities in the aortic root.

EXPERIMENTAL

MATERIALS AND METHODS

Animal protocol

The research protocol was reviewed and approved by the Committee on Animal Care, Office Vétérinaire Cantonal, Lausanne. All animals received care in compliance with the Principles of Laboratory Animal Care formulated by the National Society for Medical Research and the Guide for the Care and Use of Laboratory Animals prepared by the National Academy of Sciences and published by the National Institutes of Health, NIH Publication No. 80-23, revised in 1985.

The mean body weight of five domestic pigs was 61.2 ± 7.8 kg and mean body surface was 1.38 ± 0.13 m^2. General anaesthesia was induced with intravenous ketamine (1 mg/kg per body weight) and propofol (4.0 mg/kg per body weight) and was maintained by volatile anaesthetics (isoflurane 1.5–2.5%). The animals were equipped with a jugular central venous catheter, femoral arterial catheter for haemodynamic monitoring and five-lead electrocardiogram.

The heart was exposed via median sternotomy. The right atrium and inferior vena cava were cannulated with a 32 Fr venous cannula (SmartCannula®, Lausanne, Switzerland), and arterial cannulation at the aortic arch was done using a 20 Fr cannula (Eopa® cannula, Medtronic, Inc., Minneapolis, MN, USA). Clear priming (800 ml) and full systemic heparinization (heparin loading dose 300 units/kg per body weight with activated clotting time >480 s) were used throughout the procedure. After cross-clamping of the ascending aorta, cold crystalloid cardioplegia was administered into the aortic root. The ascending aorta was opened 1 cm superior to the SJ. Six ultrasonic crystals (Sonometrics Corp., London, ON, Canada) were implanted into the aortic root. The 2 mm high-fidelity crystals (200 Hz) were secured by 5-0 polypropylene suture at three commissures and had their projection at the AoB, which is at the deepest point of each IVT. The crystal orientation was towards the lumen of the aortic root. After the crystal electrodes were exteriorized, through the aortic incision, the aorta was closed with 4-0 polypropylene suture. High-fidelity catheter-tipped pressure transducers (Millar Instruments, Houston, TX, USA) were placed in the ascending aorta and into the left ventricular cavity to obtain the pressure. Flow was measured by a PeriVascular flow probe (Medistim ASA, Oslo, Norway) at the ascending aorta.

After the cardiopulmonary bypass was discontinued, and the animal was haemodynamically stable, five recordings of 10 min each were undertaken. Transoesophageal echocardiography was obtained to verify the competence of the aortic valve. At the end of the experiment, the heart was explanted and autopsy was performed to confirm the correct position of all six crystals.

Cardiac cycle and time-setting of measurements

Aortic root geometry was assessed over the whole cardiac cycle. According to the pressure tracings in the left ventricle and ascending aorta, the following time-related 3D geometries were defined: (i) at the end of diastole and at the beginning of the isovolemic contraction when the pressure in the left ventricle starts to rise, (ii) aortic valve opening at equalization of arterial and ventricular pressure, (iii) peak ejection, (iv) end of the systole, when the aortic valve closes and at (v) the end of the isovolaemic relaxation at the lowest pressure value in the left ventricle when the mitral valve opens.

3D geometry of the aortic root

The 3D geometry of the aortic root was defined as an oblique triangular prism in our previous reports [1, 2]. The superior triangle is positioned at the SJ, and three edges of the triangle correspond to the anterior, right and left commissures. The basal triangle is positioned at the AoB, and its edges correspond to the vertical projection of the three commissures into the AoB [1, 2]. The distance between the sinotubular and the basal markers corresponds to the height of the IVTs. The AoB and the SJ triangles are not parallel and enclose a tilt angle. The asymmetry of the aortic root is defined by one sole parameter, the aortic root vector, that defines its direction and tilt angle (Fig. 1) [1, 2].

Data acquisition and definition of 3D deformation

Measured distances in the aortic root, and the pressure in the left ventricle and in the ascending aorta were synchronized by using Digital Sonomicromter System software (Sonometric Corporation). In post-measurement processing (CardioSoft program, Sonometric Corporation), the distance between crystals, and time-related 3D reconstruction of the aortic root and the aortic root vector were defined. The following distances were measured: (i) the intercommissural distances at the SJ, (ii) basal distances between the three crystals at the AoB, (iii) the distance at the IVT and (iv) the diagonal distances corresponding to each sinus. The radius of the AoB as well of the SJ was calculated by using the rules in Euclidean space where each triangle has a circumscribed circle [10]. The volume of the aortic root was calculated according to the oblique conical frustum where the basal and the top surface are not parallel [11].

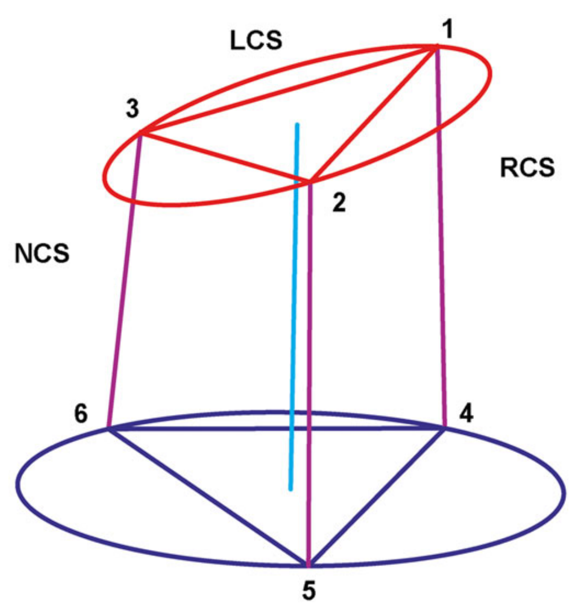

Figure 1: Geometric model of the aortic root. The '123' triangle is positioned in the sinotubular junction. The three edges correspond to the LCS, RCS and NCS commissures. The triangle at the aortic root base is marked by the '456' triangle, and the basal points correspond to the vertical projection of the three commissures into the root base. By interconnecting the points of both triangles, a model of the aortic root is obtained. This model is a prism where the basal and the sinotubular junction plane are not parallel. The axis of the prism interconnects the centre of the sinotubular junction and aortic root base. LCS: left coronary sinus; RCS: right coronary sinus; NCS: non-coronary sinus.

Definition of aortic root tilt angle and torsion

The tilt angle was computed as the angle between the normal vector of the SJ and the z-axis. The torsion angle was defined as the angle between the z-axis and the vector going through the centroids of the AoB and the SJ. The uncertainty for both of these angles was determined via a Monte-Carlo simulation: the segments of the prism were drawn from a Gaussian distribution with sample mean and variance (based on the repeated measures of each segment), the prism was reconstructed on the basis of the drawn segments and the angles were computed for the reconstructed prism. Repeating this process 1000 times, and as such having 1000 values of the torsion and the tilt angle for each prism, allowed us to generate a good statistical estimate of these quantities (Fig. 2).

Statistical analysis of measured data

Ten consecutive heartbeats from each measurement sequence (five sequences of 10 min for each animal were registered) with a minimal amount of noise were chosen for analysis. The data are presented as mean and standard deviation. The measured parameter changes were tested for significance using the Student's t-test for paired observations ($P > 0.05$ was significant). A univariate generalized linear model was used to test for significant differences ($P > 0.05$ was significant). The radius of the SJ and AoB was examined to evaluate the order of relative expansions, and values were compared with the baseline radius at the end of diastole.

Computational fluid dynamics modelling of the aortic root

A geometrical model, suitable for computational fluid dynamics (CFD) simulations, was established for the aortic root in order to evaluate pressure, velocity and shear stress profiles. The geometry was designed based on 3D real-time measurements, calculations and experimental data (Fig. 3). In particular, the dimensions of the prism were used to build eight geometrical models representative of the cardiac cycle and time-setting of measurements described previously (five characteristic steps and three additional intermediate positions). A discretized set of 100 geometrical models was interpolated and generated in order to reproduce the geometrical deformation of the aortic root and the movement of the three leaflets during the complete cardiac cycle.

The ANSYS ICEMCFD (ANSYS, Inc., Cecil Township, PA, USA) preprocessor tool was used to generate the multiblock structured grids needed by the Navier–Stokes Multi-Block (NSMB) flow solver. An O-grid topology (which aligns the hexahedral cells of the structured grid with the walls of the geometrical model) was employed to refine the mesh close to the walls in order to correctly capture the laminar boundary layer in these regions [12]. The grid for the aortic root comprises 308 structured blocks for around 1.8 million cells.

Since the simulation was performed in a large vessel, blood was modelled as a Newtonian [13, 14] fluid with a viscosity of 4.10^{-3} Pa s and a density of 1060 kg/m^3. No-slip boundary conditions were imposed on the artery walls, as well as on the valve leaflets. At the inlet of the aortic root, a pulsatile velocity flow profile was applied according to the measured values from the experimental scenario. Pressure conditions were applied at the outlet of the aortic root as well as at the outlet of the coronary arteries. The NSMB solver uses a cell-centred finite volume method to solve the compressible Navier–Stokes equations [15, 16]. The spatial discretization was ensured by a forth-order central scheme, while the time discretization was resolved by an implicit scheme.

RESULTS

Experiments were successfully performed for all five animals. The recordings were performed under stable haemodynamical conditions over 10 min, and were repeated five times. From obtained data, five consecutive heartbeats of each measurement series were chosen for analysis. Systolic pressure was 104 ± 19.3 mmHg, diastolic pressure 66 ± 20.1 mmHg and heart rate was 99 ± 13.7/min. The mean flow measured at the ascending aorta was 3.3 ± 0.38

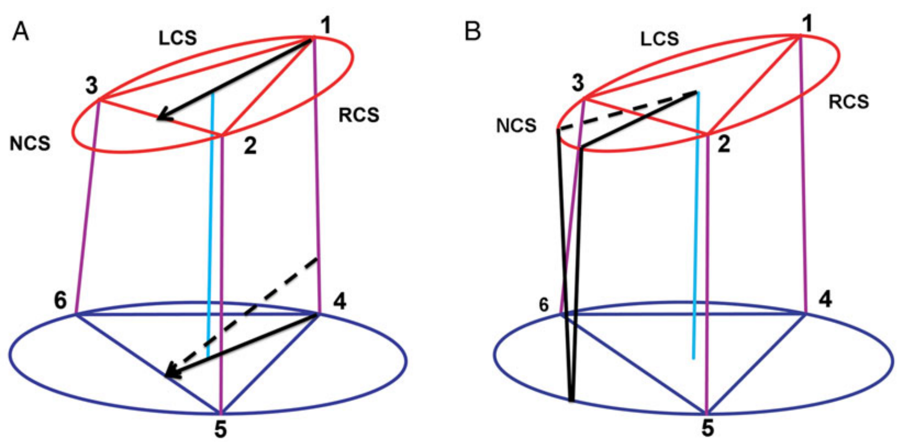

Figure 2: Aortic root tilt angle and torsion angle shown on the 3D model. The aortic root tilt angle is the angle between the sinotubular junction and aortic root base (**A**). The solid arrow in triangle '123' is a vector of the sinotubular junction. The aortic root base vector is positioned at the triangle '456'. Projecting the sinotubular junction vector onto the aortic root base (dashed line arrow), the tilt angle between two planes becomes more obvious. The aortic root torsion is twisting around the root axis, the green solid line connecting the centre of the sinotubuar junction and the aortic root base triangles (**B**). The grade of torsion is presented as the torsion angle and represents the displacement of the sinotubular junction with regard to the aortic root base. LCS: left coronary sinus; RCS: right coronary sinus; NCS: non-coronary sinus.

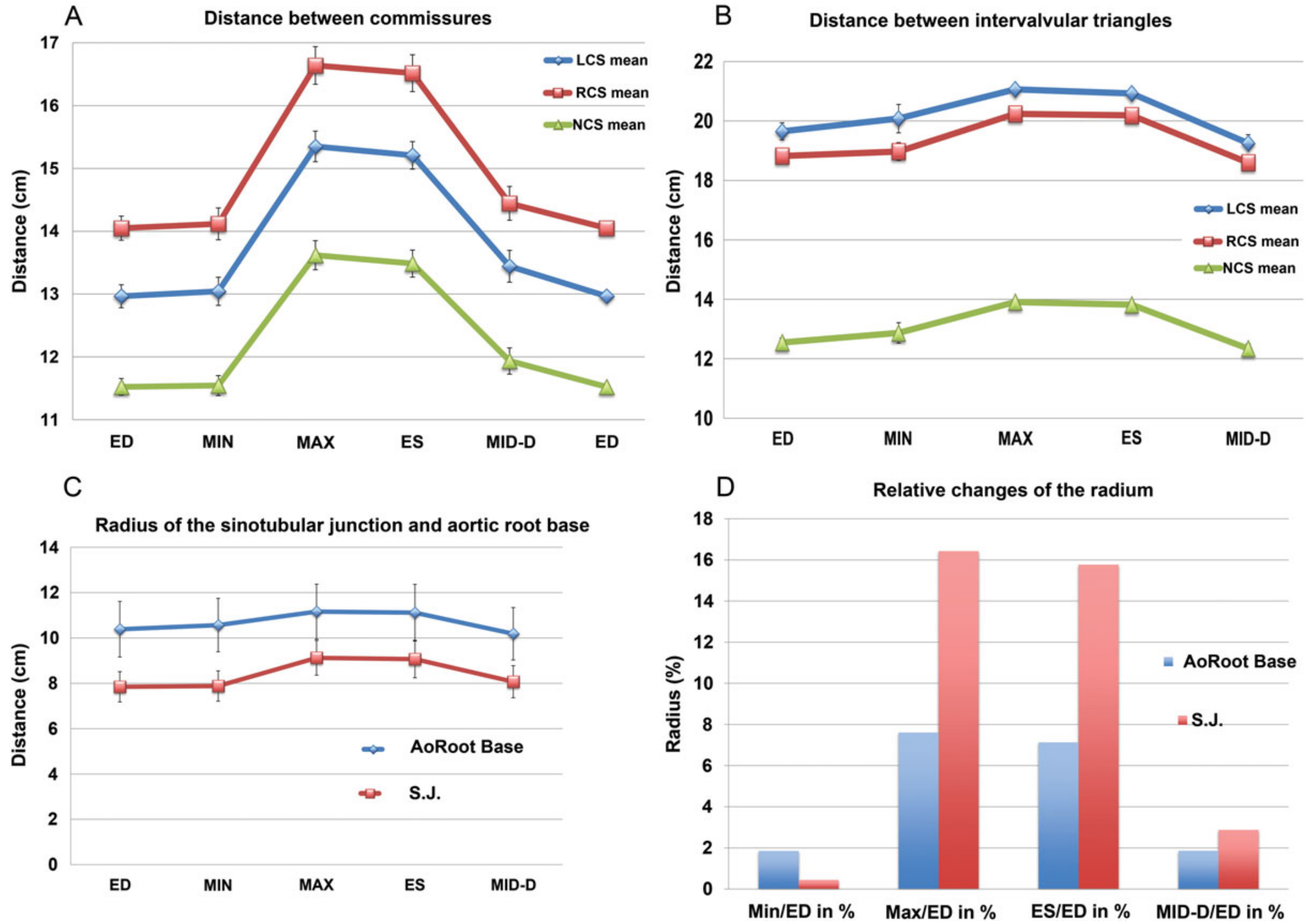

Figure 3: The distance between the three commissures (**A**), their projection at the aortic root base (**B**) and the radius of the aortic root base and the sinotubular junction (**C**) show a similar pattern. Maximal expansion was registered in the period of valve opening to peak ejection, followed by constant values till aortic valve closures and rapid increase of measured parameters during isovolaemic relaxation. The aortic root base radius is larger than the radius of the sinotubular junction (**C**); however, the relative changes of deformation were more prominent at the sinotubular junction (**D**). On the plot, the columns represent relative radius changes when compared with the end-diastolic values. The expansion of the sinotubular junction during ejection is about two times the expansion at the level of the aortic root base (**C** and **D**). SJ: sinotubular junction; AoRoot base: aortic root base; LCS: left coronary sinus; RCS: right coronary sinus; NCS: non-coronary sinus; ED: end-diastole; Min: end of the isovolaemic contraction; Max: maximal/peak ejection; ES: end of systole; Mid-D: mid-term of diastole at mitral valve opening.

l/min. There was no valve regurgitation registered during the recording, and at autopsy in all five cases, the crystals were confirmed to be in the correct positions.

3D aortic root deformation during cardiac cycle

The expansion of three sinuses at the level of commissures showed a similar pattern. The expansion of the left (LCS) and right coronary sinus (RCS) was similar over the whole cardiac cycle. Both were significantly larger than the expansion recorded in the non-coronary sinus (NCS) ($P > 0.05$). The expansion pattern was as follows: maximal expansion was registered between the end of the isovolaemic contraction at peak ejection: 13.04 ± 0.22 mm for the LCS, 14.11 ± 0.25 mm for the RCS and 11.54 ± 0.15 mm for the NCS vs 15.3 ± 0.2 mm for the LCS, 16.6 ± 0.3 mm for the RCS and 13.6 ± 0.2 mm for the NCS. This rapid expansion phase was followed by a plateau between peak ejection and closure of the aortic leaflets. There was a rapid drop in commissural distances registered during the initial phase of the diastole in the period from the closure of the aortic valve: 15.2 ± 0.26 mm for the LCS, 16.5 ± 0.26 mm for the RCS and 13.48 ± 0.21 for the NCS to the opening of the mitral valve: 13.44 ± 0.25 mm for the LCS, 14.44 ± 0.26 mm for the RCS and 11.93 ± 0.20 mm for the NCS. Minimal distance reduction was observed between the period of mitral valve closure and the beginning of the isovolaemic contraction ($P < 0.05$). A similar expansion pattern was observed at the AoB, with the only exception being a slight increase of distances during isovolaemic contraction. Expansion of the LCS and RCS base was identical and larger than the expansion of the NCS base ($P > 0.05$). Maximal expansion was registered between the period of aortic valve opening and peak ejection with: 20.07 ± 0.47 mm for the LCS, 18.97 ± 0.29 mm for the RCS and 12.87 ± 0.34 mm for the NCS vs 21.06 ± 0.13 mm for the LCS, 20.23 ± 0.14 mm for the RCS and 13.82 ± 0.08 for the NCS. A rapid drop in basal distances was registered in the period from the closure of the aortic valve and the opening of the mitral valve: 20.92 ± 0.19 mm for the LCS, 20.18 ± 0.22 mm for the RCS and 13.82 ± 0.11 mm for the NCS vs 19.24 ± 0.28 mm for the LCS, 18.59 ± 0.17 mm for the RCS and 12.33 ± 0.16 mm for the NCS. From here on, all three distances measured at the AoB were slightly increasing to the level measured at the end of diastole (Table 1, Fig. 3).

The radius of the AoB was larger compared with the radius of the SJ over the whole cardiac cycle ($P < 0.05$). However, the amplitude of SJ radius deformation was larger than the deformation at the AoB ($P < 0.05$). The largest expansion for both regions was at peak ejection: 16.42 ± 6.36% for the SJ and 7.6 ± 2.52% for the AoB, followed by expansion at the end of systole: 15.77 ± 7.00% for the SJ and 7.13 ± 2.68% for the AoB when compared with the radius at the end of diastole. The smallest change of radius expansion was registered at the end of the isovolaemic contraction: 0.44 ± 0.15% for the SJ and 1.85 ± 2.45% for the AoB, when compared with the radius at the end of diastole (Table 1, Fig. 3).

The geometrical deformation of the IVTs was as follows: the largest dimensions were measured at the left (LIVT) followed by anterior (AIVT) and at the right (RIVT) ($P > 0.05$). All three distances showed almost a linear expansion from the beginning of the isovolaemic contraction at 16.18 ± 0.04 mm for the LIVT, 14.38 ± 0.04 mm for the AIVT and 12.94 ± 0.04 mm for the RIVT to the peak ejection: 16.38 ± 0.06 mm for the LIVT, 14.49 ± 0.06 mm for the AIVT and 13.01 ± 0.07 mm for the RIVT. A plateau followed till the closure of the aortic valve: 16.38 ± 0.06 mm for the LIVT, 14.49 ± 0.06 mm for the AIVT and 13.01 ± 0.07 mm for the RIVT, and a decrease in distances during the isovolaemic phase of diastole: 16.17 ± 0.05 mm for the LIVT, 14.41 ± 0.06 mm for the AIVT and 12.96 ± 0.06 mm for the RIVT.

aortic root volume showed a slight increase at isovolaemic contraction from 4.28 ± 0.15 ml at the end of diastole to 4.45 ± 0.15 ml at the end of isovolaemic contraction. From here on, the volume increased to 5.15 ± 0.18 ml at peak ejection and 5.10 ± 0.18 ml at the closure of the valve. Then the volume decreased down to a minimal value of 4.22 ± 0.15 ml at the time of mitral valve opening (Table 2).

The tilt angle (α) of the aortic root is the angle between the SJ and AoB and corresponds to the aortic root vector tilt angle. The

Table 1: Measured distances at the three commissures, aortic root base and intervalvular triangles

	ED	Min	MaxE	ES	Mid-D
Intercommissural distance (mm)					
LCS	12.96 ± 0.18	13.04 ± 0.22	15.35 ± 0.24	15.20 ± 0.21	13.44 ± 0.25
RCS	14.05 ± 0.19	14.11 ± 0.25	16.54 ± 0.3	16.51 ± 0.29	14.44 ± 0.27
NCS	11.52 ± 0.13	11.54 ± 0.15	13.61 ± 0.23	13.48 ± 0.21	11.93 ± 0.13
Distance at the aortic root base (mm)					
LCS	19.65 ± 0.28	20.07 ± 0.47	21.06 ± 0.14	20.93 ± 0.19	19.25 ± 0.28
RCS	18.82 ± 0.17	18.97 ± 0.29	20.23 ± 0.14	20.18 ± 0.22	18.59 ± 0.17
NCS	12.54 ± 0.14	12.87 ± 0.34	13.90 ± 0.08	12.82 ± 0.11	12.33 ± 0.16
Sinotubular junction and aortic root base radius (mm)					
SJ	7.84 ± 0.69	7.87 ± 0.69	9.12 ± 0.76	9.06 ± 0.82	8.07 ± 0.28
AoB	10.38 ± 1.22	10.57 ± 1.18	11.16 ± 1.21	11.11 ± 1.25	10.18 ± 1.15
	ED/ED	Min/ED	MaxE/ED	ES/ED	Mid-D/ED
Relative radius change when compared with the ED radius					
SJ	1	0.44 ± 1.15%	16.42 ± 6.36%	15.77 ± 7.0%	2.87 ± 1.62%
AoB	1	1.85 ± 1.45%	7.6 ± 2.52%	7.13 ± 2.68%	1.85 ± 1.79%

Additionally, the radii of the sinotubular junction and of the aortic root base were calculated. Relative expansion of the radius when compared with the end-diastolic value is also presented.
LCS: left coronary sinus; RCS: right coronary sinus; NCS: non-coronary sinus; ED: end-diastole; Min: end of the isovolaemic contraction; MaxE: maximal/peak ejection; ES: end of systole; Mid-D: mid-term of diastole at mitral valve opening.

Table 2: The tilt angle and rotation angle of the aortic root

Aortic root tilt and torsion angle (Grade°)	ED	Min	MaxE	ES	Mid-D
Tilt angle α	17.78 ± 8.43	18.37 ± 8.01	15.01 ± 7.39	15.24 ± 8.13	16.87 ± 8.94
Torsion angle β	21.24 ± 2.10	21.72 ± 1.93	18.34 ± 1.94	18.78 ± 3.13	20.12 ± 1.80
Relative aortic root volume change when compared with the ED volume					
Volume (ml)	4.28 ± 0.15	4.45 ± 0.15	5.15 ± 0.18	5.10 ± 0.18	4.22 ± 0.14
	ED/ED	Min/ED	MaxE/ED	ES/ED	Mid-D/ED
Ratio (%)	1	4.82 ± 0.39	21.37 ± 0.14%	19.76 ± 0.14%	0.3 ± 0.85%

Aortic root volume is presented in absolute as well in relative values. For relative values, the end-diastolic value was considered as baseline. Data are presented as mean ± standard deviation.
ED: end-diastole; Min: end of the isovolaemic contraction; MaxE: maximal/peak ejection; ES: end of systole; Mid-D: mid-term of diastole at mitral valve opening.

EXPERIMENTAL

rotation or the torsion angle (β) was determined as twist of the SJ and AoB planes and corresponds to the displacement of the root vector in a vertical plane. The tilt angle α at the end of diastole was 17.78 ± 8.43° and slightly increased to 18.37 ± 8.01° at the end of isovolaemic contraction. From here on, the tilt angle showed a drop during the ejection phase and was 15.01 ± 7.93° at peak ejection and 15.24 ± 8.13° at the closure of the aortic valve. From here on, the tilt angle increased and reached 16.87 ± 8.94° at the end of isovolaemic diastole. The same phenomenon was noted for the torsion angle β, which at the end of diastole was 21.24 ± 2.09°, and increased to 21.72 ± 1.93° at the end of isovolaemic contraction. From here on, there was a decrease of rotation angle noted, with 18.34 ± 1.94° at peak ejection and 18.78 ± 3.13° at closure of the aortic valve. The rotation angle again increased at the opening of the mitral valve to 20.12 ± 1.80° (Table 2, Fig. 4).

Computational fluid dynamics analysis of the aortic root

Shear stress and the local pressure profile were investigated at leaflets, at IVTs as well as on the wall of the sinuses. At the end of diastole, the bodies of the three leaflets, the hinge regions of the leaflets and the IVTs were exposed to low shear stress in a range of 0–8 Pa. High shear stress on the lunula was found in the range of >45 Pa. During isovolaemic contraction, there was only slight shear stress augmentation registered at the leaflet body and IVTs with a range of 10–28 Pa. The hinge areas remained in low shear stress (range 0–8 Pa) and the lunula in high shear stress regions at >60 Pa. At peak ejection, the lunula as well the three commissures were exposed to high shear stress (range >40–32 Pa). At the leaflet body the shear stress progressively decreased from the lunular region towards the hinge area. Moderately high shear stress (36–28 Pa) was registered just underneath the lunula and there was moderately low shear stress (24–12 Pa) at the basal regions of the leaflet body. The hinge area remained in a low shear stress (range 0–8 Pa) region. This was the same for the IVT, where the superior half was exposed to moderate shear stress (28–12 Pa) and the inferior half to low shear stress (0–8 Pa). At the end of systole, the leaflet body was again exposed to a low shear stress area (range 0–8 Pa), with the exception of the regions underneath the valve coaptation, which had moderately high shear stress (range 20–28 Pa). The lunula was in a constant high shear stress region. The IVT were in a low shear stress area (0–4 Pa). The wall of the three sinuses during the whole cardiac cycle was exposed to low shear stress (0–8 Pa) (Fig. 5, Videos 1 and 2).

At the end of diastole, low pressure (75–85 mmHg) was present at the leaflet coaptation and bodies of the leaflets, while nadirs and IVTs were in moderately high-pressure areas (92–95 mmHg). At the end of isovolaemic contraction, the nadirs remain in low-pressure areas (75–85 mmHg). Meanwhile, the central portion of the leaflets as well the superior two-thirds of the IVT and the part belonging to the attachment of leaflets were in high-pressure regions (>120 mmHg). The rest of the leaflets and hinge area were in moderately high-pressure regions (92–97.5 mmHg). At peak ejection, the lunula and superior half of the leaflets were exposed to low pressure (75–85 mmHg). The inferior half of the leaflet body was exposed to moderately high pressure (90–97.5 mmHg). At closure of the aortic valve, as well as during diastole, the leaflets as well as their nadirs were exposed to moderate pressure (80–90 mmHg). At the end of systole and during diastole, the IVTs were exposed to moderate pressure (80–90 mmHg) (Fig. 5, Videos 1 and 2).

DISCUSSION

The aortic root has a complex morphological structure, with strict spatial arrangement of its components. The general conviction is that the aortic root has a symmetric structure where the three sinuses, the IVTs and the three leaflets are equal in size [17, 18]. This simple interpretation of the aortic root morphology is a well-accepted interpretation and is used as a bench model in a majority of haemodynamics studies evaluating local shear stress conditions of the native aortic root as well of synthetic aortic root structures [4, 5, 19, 20]. In fact, the components of the aortic root have shape differences that result in an asymmetric morphology of the aortic root. It is easy to recognize that each component of this highly sophisticated structure contributes to an optimal 3D architecture and function. Providing a path for large-volume blood flow during the ejection and at the same time ascertaining laminar flow with minimal resistance and less possible tissue stress and damage. It is easy to recognize that this complex task may be accomplished only by precise synchronized function of all aortic root components. The well-coordinated spatial

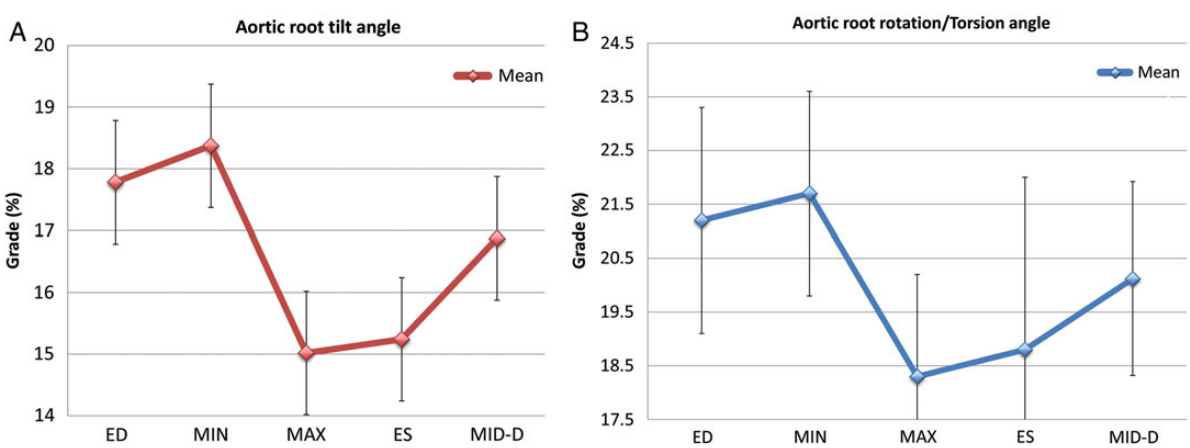

Figure 4: Plot of the aortic root tilt angle (**A**) and aortic root torsion angle (**B**). The changes of both angles during the cardiac cycle show a similar pattern. The maximal tilt angle and the rotation angle were measured at the end of the isovolaemic contraction, just prior to valve opening. The lowest values were registered at peak ejection; from here on, the aortic root tilt angle and rotation angle increased. ED: end-diastole; Min: end of the isovolaemic contraction; Max: maximal/peak ejection; ES: end of systole; Mid-D: mid-term of diastole at mitral valve opening.

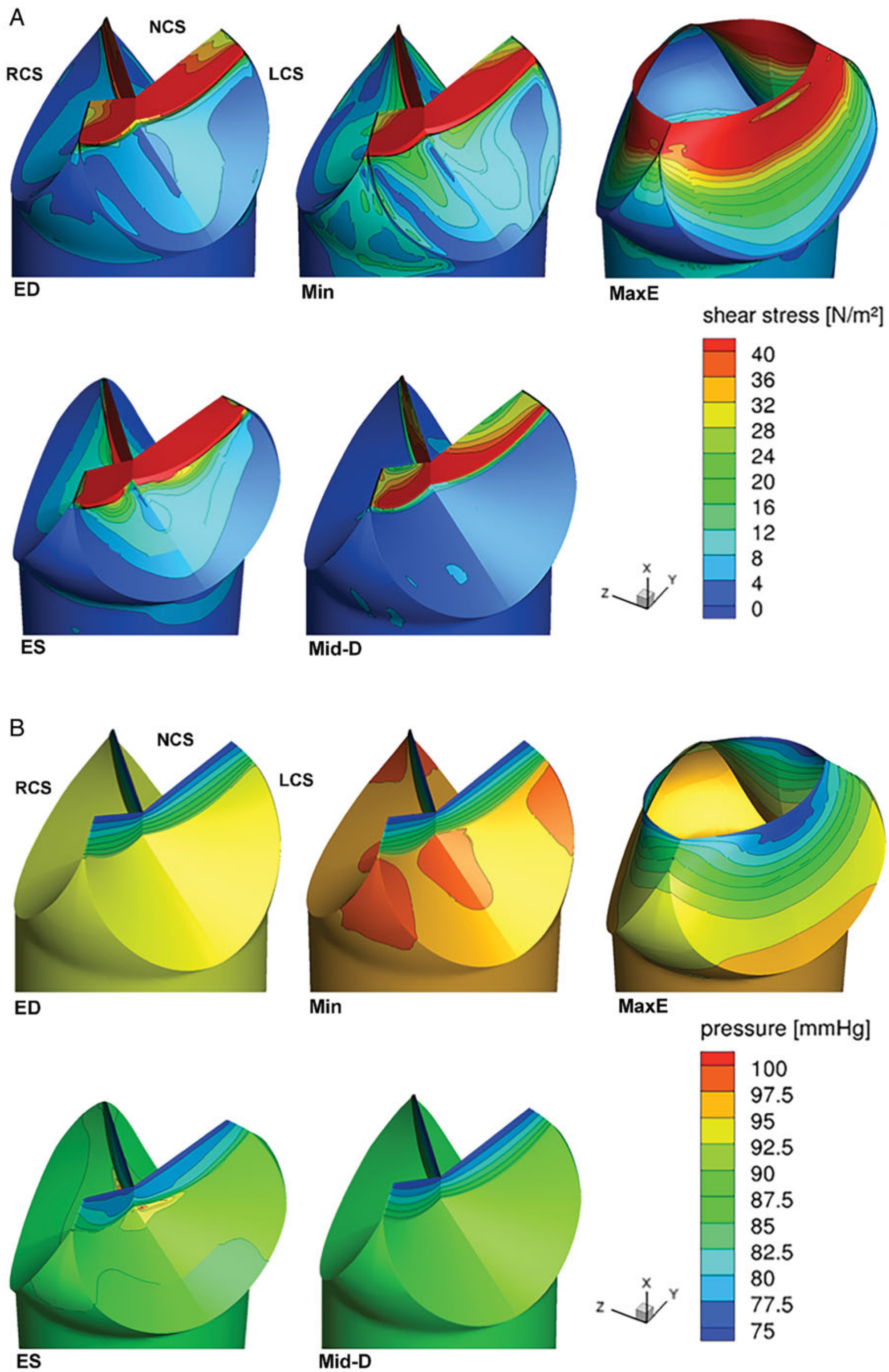

Figure 5: Local shear stress and pressure profile of the aortic valve, intervalvular triangles and aortic root base. Local pressure changes during the cardiac cycle are seen on (**A**), and the shear stress profile on (**B**). At the end of the isovolaemic contraction, pressure augmentation was noted; at this point, the shear stress was in moderately low ranges. At peak ejection, high shear stress was noted at the superior one-third of the leaflet body and intervalvular triangles. ED: end-diastole; Min: end of the isovolaemic contraction; Max: maximal/peak ejection; ES: end of systole; Mid-D: mid-term of diastole at mitral valve opening; LCS: left coronary sinus; RCS: right coronary sinus; NCS: non-coronary sinus.

behaviour of aortic root elements and their combined impact on haemodynamics was well described by Lansac *et al*. [6, 7]. Aortic root shape change during the cardiac cycle was postulated as being a shock absorber during systole that reduces shear stress on the leaflets [6]. Unfortunately, a computed fluid dynamics model was not applied in order to support their suggestion [6, 7].

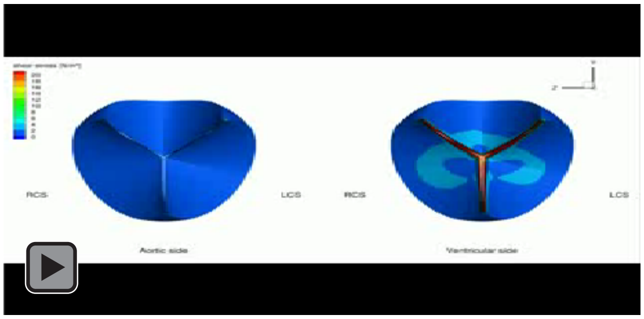

Video 1: Showing the shear stress dynamics during the cardiac cycle; note that the valve is seen from the ventricular as well as the aortic side. Constant low shear stress exposure on the aortic surface is noted.

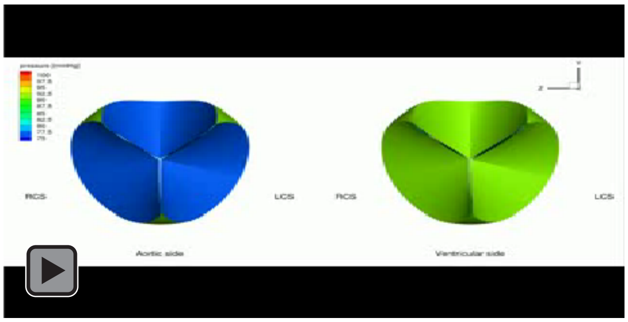

Video 2: Showing the pressure dynamics during the cardiac cycle, note that the valve is seen from the ventricular as well as the aortic side. Constant low-pressure exposure on the aortic surface is noted.

In recent work, aortic root deformation was defined by using a previously described 3D geometrical model of the aortic root. This model was based on natural aortic root asymmetry and follows the precise spatial patterns of the sinuses of Valsava, IVTs and three leaflets [1, 2]. The 3D model is presented as a prism, and is a numerical and geometrical interpretation of natural aortic root architectures [1, 2]. In recent work, this 3D geometry was used in order to describe spatial deformation of all root components and to determine the local haemodynamics under physiological conditions. Indeed our results on aortic root geometrical deformation are in a certain way similar to those obtained by Lansac [6, 7]. In our geometry not only the three sinuses were included [6, 7], but we also considered the deformation of IVTs, AoB and SJ. Doing so, we were able to determine the deformation of the aortic root including its components that physiologically belong to two different compartments: the left ventricle and the aorta. Doing so, we also determined the behaviour of the aortic root 'in total' and defined the tilt angle and rotation angle of the aortic root during the cardiac cycle. This to the best of our knowledge has not been described until now.

aortic root tilt angle and torsion angle changes showed a similar pattern that was the inverse of the expansion of the AoB and the SJ. During systole, the tilt angle as well the torsion angle decreased, and during diastole both angles increased. The tilt angle reduction during ejection brings the planes of the SJ and the AoB into a more parallel position and the aortic root becomes more cylindrical in shape. As a consequence, the SJ is almost in a parallel position to the outflow tract of the left ventricle during the ejection phase. The reduction of the torsion angle during ejection rotates the aortic root from the left to a more right and neutral position, and back during diastole. It appears that changes in aortic root tilt and torsion angle exert a crucial influence on aortic root 3D anatomy. The reduction during ejection results in the aortic root geometry being closer to a cylindrical shape and the increase of angles during diastole results in the aortic root becoming a frustum, where the two planes enclose a tilt angle in the horizontal plane.

The impact of aortic root geometry deformation from a frustum to cylinder on local pressure and under flow shear stress conditions was evaluated in a CFD model. The cylindrical geometry, identified in a period from valve opening to valve closure aligns the aortic root in a straight line with the ascending aorta and left ventricular outflow tract. This quasistraight alignment facilitates blood ejection from the left ventricle to the ascending aorta and may be considered as an 'energy release' form. In real-time CFD simulation based on our 3D aortic root geometry reconstruction, there was a presence of low shear stress areas in a majority of the aortic root components such as at the IVTs, leaflet bodies, valve nadirs and the left ventricular outflow tract. After the aortic valve closes, the tilt angle and the rotation angle constantly increase to their maximal value at the end of the isovolaemic contraction. At this point, the aortic root shape regains its frustum-like geometry. The frustum-like shape, in contrast to the cylindrical form, may be interpreted as an 'energy storage' condition. Namely, from closure of the aortic valve to the end of diastole, there is an important increase of shear stress and pressure observed at the three leaflets, IVTs and at the valve nadirs. This systematic and well-organized repetitive aortic root geometry change conjoined with shear stress and the pressure alteration may be plotted as a cyclic alteration of 'energy release' and 'energy accumulation'. The geometry during diastole with augmentation of the torsion and tilt angle accumulates the energy from the hydrostatic pressure of the blood in the into the aortic root wall tension. At ejection the aortic root becomes untwisted and the release of conserved and accumulated elastic energy facilitates blood propulsion from the left ventricle up into the ascending aorta. However, this, though at first gaze seems a very simple concept, should be proved by further investigations.

Limitations of the study

It may be argued that the clinical implication, due to the experimental nature of the recent report, is of minimal value. However, it is a fact that in this work we provided a very simple numerical interpretation of complex 3D aortic root dynamics. Our approach to define the aortic root physiology has to be considered as a bench model that provides us with a better understanding of native aortic root physiology. Further, it can be used for comparative analysis of native and synthetic structures in order to better understand the different root reconstructive procedures and predict their outcome. In this way, not only we may better understand the root physiology but also we can individualize the reconstructive procedure and optimize the outcome. However, the way to go is still long and, in future, further experimental as well clinical studies have to be still performed.

Funding

This study was supported by the research Grant of Swiss Heart Foundation, Bern, Switzerland.

Conflict of interest: none declared.

REFERENCES

[1] Berdajs D, Patonay L, Turina M. Clinical anatomy of the aortic root. Cardiovasc Surg 2002;10:320–7.

[2] Berdajs D, Zund G, Schurr U, Camenisch C, Turina MI, Genoni M. Geometric models of aortic and pulmonary roots: suggestion for Ross procedure. Eur J Cardiothoracic Surg 2007;31:31–5.

[3] Sutton JP III, Ho SY, Anderson RH. The forgotten interleaflet triangles: a review of the surgical anatomy of the aortic valve. Ann Thorac Surg 1995;59:419–27.

[4] Robicsek F, Thubrikar MJ. Role of sinus wall compliance in aortic leaflet function. Am J Cardiol 1999;84:944–6, A7.

[5] Beck A, Thubrikar MJ, Robicsek F. Stress analysis of the aortic valve with and without the sinuses of valsalva. J Heart Valve Dis 2001;10:1–11.

[6] Lansac E, Lim HS, Shomura Y, Lim KH, Rice NT, Goetz WA *et al*. Aortic root dynamics are asymmetric. J Heart Valve Dis 2005;14:400–7.

[7] Lansac E, Lim HS, Shomura Y, Lim KH, Rice NT, Goetz WA *et al*. A four-dimensional study of the aortic root dynamics. Eur J Cardiothorac Surg 2002;22:497–503.

[8] David TE, Armstrong S, Manlhiot C, McCrindle BW, Feindel CM. Long-term results of aortic root repair using the reimplantation technique. J Thorac Cardiovasc Surg 2013;145:S22–5.

[9] David TE. Aortic valve sparing operations: outcomes at 20 years. Ann Cardiothorac Surg 2013;2:24–9.

[10] Dörrie H. 100 Great Problems of Elementary Mathematics. Dover: Dover Publications, 1965.

[11] Weisstein EW. 'Conical Frustum.' From MathWorld—A Wolfram Web Resource.

[12] Liseikin VD. Grid Generation Methods, 2nd edn. Heidelberg: Springer, 2010, 18–29.

[13] Vasava P, Jalali P, Dabagh M, Kolari PJ. Finite element modelling of pulsatile blood flow in idealized model of human aortic arch: study of hypotension and hypertension. Comput Math Methods Med 2012;Article ID 861837:1–14.

[14] Khanafer KM, Gadhoke P, Berguer R, Bull JL. Modeling pulsatile flow in aortic aneurysms: effect of non-Newtonian properties of blood. Biorheology 2005;43:661–79.

[15] Vos JB, Leyland P, van Kemenade V, Gacherieu C, Duquesne N, Lötstedt P. NSMB Handbook 6.07, 2014, 601–97.

[16] Vos J, Rizzi A, Corjon A, Chaput E, Soinne E. Recent advances in aerodynamics inside the NSMB (Navier-Stokes Multi-Block) consortium. AIAA Paper 1998;802:1998–99.

[17] Anderson RH. Clinical anatomy of the aortic root. Heart 2000;84:670–3.

[18] Misfeld M, Sievers HH. Heart valve macro- and microstructure. Philos Trans R Soc Lond B Biol Sci 2007;362:1421–36.

[19] Soncini M, Votta E, Zinicchino S, Burrone V, Mangini A, Lemma M. *et al*. Aortic root performance after valve sparing procedure: a comparative finite element analysis. Med Eng Phys 2009;31:234–43.

[20] Kunzelman KS, Grande J, David TE, Cochran RP, Verrier E. Aortic root and valve relationships: impact on surgical repair. J Thorac Cardiovasc Surg 1994;107:162–70.